Scientific Research Publishing

Structure Refinement of Mn-Substituted LiMn$_x$Fe$_{1-x}$PO$_4$

Masakazu Togo, Atsushi Nakahira

Department of Materials Science, Graduate School of Osaka Prefecture University, Osaka, Japan
Email: nakahira@mtr.osakafu-u.ac.jp

Abstract

For Mn substituted LiMn$_x$Fe$_{1-x}$PO$_4$ synthesized by hydrothermal process, the structural differences caused by Mn substitution were characterized by SEM, ICP, XRD, XAFS, and FT-IR. In this study, by using XAFS advantageous to the atomic selectivity, the local structure of MeO$_6$ octahedral was investigated. From ICP, Mn composition in the products was similar to Mn addition amount, and the peak shifts of XRD patterns with increasing Mn addition were observed. The lattice constants refined by Rietveld analysis were $a = 1.0338 \pm 5$ nm, $b = 0.5995 \pm 4$ nm and $c = 0.4696 \pm 1$ nm in LiFePO$_4$, and it was expanded linearly with increasing Mn addition. Fe-O bond distance, which was calculated by curve fitting of the radius distribution function of LiMn$_x$Fe$_{1-x}$PO$_4$, was 0.208 nm smaller than 0.214 nm of Mn-O bond. In addition, MeO$_6$ octahedral expansion was affected to PO$_4$ vibrational structure from FT-IR spectra.

Keywords

Lithium Ion Battery, Olivine Material, Local Structure, Mn Substitution

1. Introduction

The development of energy storage technique leads to comfortable life. Lithium ion battery (LIB) having high energy density is applied for mobile devices, electric vehicle and storage devices of sustainable energy. With expanding the demands of LIB, there are some problems to be solved. As one of major problems, Co concluded in the cathode material is expensive and poor resource. In order to reduce battery costs, especially, the alternative electrode material to LiCoO$_2$ is needed. LiMnO$_2$ and LiFePO$_4$ are attracted as the alternative material. The electrode material cost is reduced by the usage of abundant material in resource, like Fe or Mn [1]. In addition, PO$_4$ tetrahedron consisted of strongly covalent bond

prevents oxygen decomposition during high charging state. Its structure makes a contribution to safety. Therefore, $LiFePO_4$ is suitable for mass production with the demand expansion and also for safety electrode material.

$LiFePO_4$ has olivine-type structure and belongs to poly-anion group. Padhi reported that poly-anion group material showed reversible Li ion extraction characters and olivine-type $LiFePO_4$ had higher potential than that of the other poly-anion groups [1]. $LiFePO_4$ is interesting because of its low-cost, flat-voltage characters, good cyclability and good stability. Olivine-type material, that composition expressed in $LiMePO_4$ (Me = Fe, Mn, Co. Ni), is composed of edge-shearing PO_4 tetrahedral and MeO_6 octahedral. The covalence P-O bonds in the $LiFePO_4$ structure stabilizes Fe(3d)-O(2p) anti-bond, as a result, the redox potential of Fe^{2+}/Fe^{3+} increases to higher level [1]. The redox potential is 3.4 V vs. Li^+/Li in $LiFePO_4$ and 4.1 V vs. Li^+/Li in $LiMnPO_4$ [2], respectively. In the case of Co or Ni, it is expected to have higher redox voltage. However, low Li ion diffusion character is the problem for practical usage, especially for Co and Ni [3]. By substituting the multiply-charged ion, the improvements of the various electric behaviors were reported [4] [5] [6] [7]. The Zr substituted to *Me* is efficient to prevent the degradation of capacity [8]. In this way, metal ion substitution is efficient to the improvement of the electric property. Padhi reported that Mn-O-Fe interactions in $LiMn_{0.5}Fe_{0.5}PO_4$ set the redox energy of Mn^{2+}/Mn^{3+} higher than that of Fe^{2+}/Fe^{3+} [1]. In addition, in $LiMn_{0.4}Fe_{0.6}PO_4$, Yamada reported the influence of Mn in the redox mechanism [9]. Because $LiMn_xFe_{1-x}PO_4$ has interesting features of two different plateaus (3.5 and 4.1 V), more energy density than that of pure $LiFePO_4$ is obtained.

Since then, many researchers have evaluated the electrical properties of $LiFePO_4$ [10] [11] [12] [13] [14]. The conductivity has considered being a problem of $LiFePO_4$. As one of the solutions for its problem, the addition of conduction assistant like carbon coating was reported [15] [16], and the capacity of $LiFePO_4$ at high rate was also improved. On the other hand, the morphology and crystallinity of $LiFePO_4$, which affect to the electrical property, change according to each synthesis method. The products synthesized by solid state reaction have high crystallinity relatively. The finer products synthesized by hydrothermal method are obtained, and its crystallinity tends to depend on synthesis temperature because of presence of amorphous phase or the vacancy of Li site [17]. This lack of Li is directly related to the electric property. It reported that the products hydrothermally synthesized at the temperature over 180˚C showed good property, when the hydrothermal conditions of olivine material were optimized [17] [18]. In addition, in order to decrease these influences during electric measurement, olivine materials are heat treated in inert atmosphere. Thus, in the case of hydrothermal process, the both influence of synthesis condition and Mn addition to olivine structure should be considered.

In this study, the structure of Mn substituted $LiMn_xFe_{1-x}PO_4$ synthesized by hydrothermal method was evaluated in detail. Substitution of larger size Mn^{2+}

ion is expected to distort the olivine-type structure. As more details, the structural characters of MeO_6 can be observed selectively from XAFS analysis with changing X-ray energy. Then, the effect of Mn addition on the local structure was also examined by XAFS.

2. Experimental Procedure

2.1. Synthesis of LiMn$_x$Fe$_{1-x}$PO$_4$

LiOH·H$_2$O, (NH$_4$)$_2$HPO$_4$, FeSO$_4$·7H$_2$O, MnSO$_4$·5H$_2$O (Wako. Ltd.) were used as starting materials. They were dissolved in deionized water, and 1M LiOH, 0.5 M (NH$_4$) HPO$_4$, 0.5M FeSO$_4$, 0.5M MnSO$_4$ were prepared. These reagents were weighted with molar ratio Li:P:Fe:Mn = 2:1:1-x:x (x = 0 - 1) by 0.25, respectively. In order to prevent the oxidation of Fe^{2+} to Fe^{3+}, distilled water was bubbled by N$_2$ gas, and the synthesis was done under N$_2$ atmosphere. Reagents were mixed in Teflon vessel vigorously. Teflon vessel with mixed solution was hydrothermally treated at 200°C for 24 hours. Obtained products were filtrated, washed, and dried under vacuum for overnight.

2.2. Characterization

The crystal phase of samples was identified by XRD (Ultima IV, Rigaku Co., Japan) at 2θ = 10° - 70° with scan rate of 4°/min using CuKα radiation. The microstructure was observed by FE-SEM (S-4500, Hitachi, Japan) with applied voltage of 10 kV. The specific surface area was measured by nitrogen BET method (BELSORP-mini, microtrac-BEL, Japan) using the data of P/P_0 = 10^{-3} - 10^{-2}. The Rietveld refinement of structural parameter was performed by the analysis software RIETAN-FP [19]. The refined data range was 2θ = 10° - 90° by stepping 0.01°. The composition of the sample was analyzed by ICP (PS-7800, Hitachi Co.). The sample was dissolved in 0.1 M nitric acid, and its solution was measured. The local structure of samples was investigated by XAFS spectra for Fe K-edge and MnK-edge. XAFS data were corrected by transmission mode using Si (111) double crystal monochrometer at BL14B2 in the SPring-8. For the XAFS measurement, the sample was prepared as pellets with the thickness varied to obtain a 0.5 - 1.0 jump at the both Fe K-edge and MnK-edge. The evaluation of XAFS data was conducted using the commercial software "REX2000" (RigakuCo. Ltd., Japan). The vibrational structure was identified by FT-IR (ALPHA-OPT, Bruker Co.) at wave vector range 400 - 4000 cm^{-1}. For FT-IR measurements, the sample was grinded with KBr, and the powder was pressed in a mechanical press to form a translucent pellet.

3. Results and Discussion

3.1. The Microstructure and the Composition

Mn substituted LiMn$_x$Fe$_{1-x}$PO$_4$ was synthesized by hydrothermal process at 200°C for 24 h. SEM images of the products of Mn substituted LiMn$_x$Fe$_{1-x}$PO$_4$ were shown in Figure 1. The microstructure of the products was finely plate-like
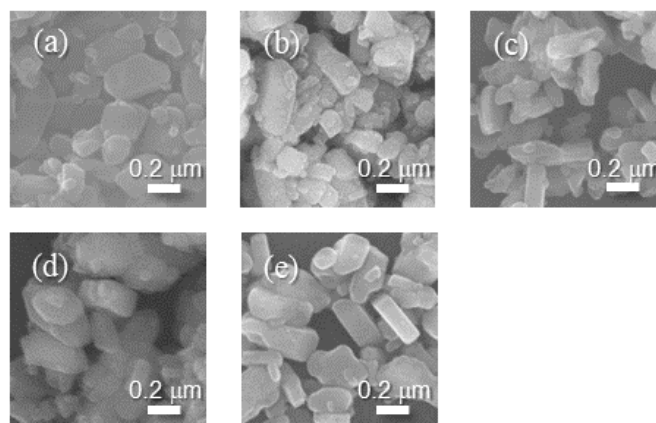
Figure 1. SEM images of the products synthesized by hydrothermal process with Mn addition ratio (a) $x = 0$, (b) $x = 0.25$, (c) $x = 0.5$, (d) $x = 0.75$, (e) $x = 1.0$.

with particle size of about 0.5 μm. In case of Mn addition, the same size particle was observed as LiFePO$_4$, and a specific surface area was about 7.8 m^2/g. No remarkable difference of the microstructure was observed regardless of Mn addition. The composition of the Mn added products was measured by ICP analysis and shown in Table 1. The ratio x of Mn addition amount was changed from 0 to 1.0 by 0.25. Compared to the ratio x of Mnaddition amount, the Mn/Fe ratio was provided equally, respectively. In addition, Li/(Mn + Fe) ratio was around 0.96 a little less than stoichiometric ratio. Therefore, it was thought that added Mn alternative to Fe was included in the products.

3.2. Structure Refinement of Mn Substituted Olivine Material

The crystal phases of the products were identified by XRD and the structure parameter was analyzed by Rietveld refinement. XRD results of the products were shown in Figure 2. The diffraction peaks were attributed to orthorhombic olivine-type structure, *Pnma*. No other crystalline peaks, which were attributed to the impurities like Fe$_2$P or Li$_3$PO$_4$, were observed. With increasing the Mn addition amount, the diffraction peaks were shifted to low angle. The Fe^{2+} ionic radius in coordination number 6 is 61 pm, and the Mn^{2+} ionic radius in coordination number 6 is 81 pm [20]. As a reason of peak shift, the lattice spacing was expanded by substituted Mn ion into olivine-structure, of which ionic radius is larger than that of Fe^{2+}. Therefore, it was thought that Mn ion was substituted with Fe ion. The refined lattice constant and the reliability factors (R-factors) were shown in Table 2. Refinement patterns of LiMn$_x$Fe$_{1-x}$PO$_4$ were shown in supplementary file. Mn was considered to be the substitute atom to Fe site, and its occupancy rate was set the stoichiometric value. Isotropic displacement parameter, B parameter, was set the constant value because of having strongly correlation with occupancy rate. In $x = 0$, R-factors was $R_{wp} = 0.53\%$, $R_p = 0.38\%$, $R_B = 2.71\%$, $R_F = 1.21\%$ and $S = 1.31\%$. According to R-factors, the calculated pattern was the good agreement with the experiment pattern. The lattice constant

Table 1. The composition of $LiMn_xFe_{1-x}PO_4$.

Elements	weight %			molecule %				
	Li	Mn	Fe	Li	Mn	Fe	Li/(Fe + Mn)	Mn/Fe
$LiMn_{0.25}Fe_{0.75}PO_4$	4.56	9.43	28.8	15.1	3.94	11.8	0.96	0.33
$LiMn_{0.50}Fe_{0.50}PO_4$	4.52	19.0	19.5	15.0	7.96	8.03	0.94	1.0
$LiMn_{0.75}Fe_{0.25}PO_4$	4.55	28.3	9.56	15.0	11.8	3.91	0.96	3.0

Table 2. The refined lattice constant and reliability factors of $LiMn_xFe_{1-x}PO_4$ by Rietveld analysis.

	Lattice parameters				Reliability factors			
	a (nm)	b (nm)	c (nm)	V	R_{wp}	R_p	R_B	R_F
$LiFePO_4$	1.0338 ± 5	0.5995 ± 4	0.4696 ± 1	0.2910 ± 8	0.53	0.38	2.71	1.21
$LiMn_{0.25}Fe_{0.25}PO_4$	1.0350 ± 5	0.6004 ± 8	0.4701 ± 3	0.2922 ± 2	0.89	0.60	3.66	1.82
$LiMn_{0.5}Fe_{0.5}PO_4$	1.0396 ± 7	0.6044 ± 7	0.4723 ± 9	0.2968 ± 7	0.84	0.58	3.45	1.36
$LiMn_{0.75}Fe_{0.25}PO_4$	1.0403 ± 9	0.6060 ± 9	0.4727 ± 3	0.2980 ± 9	1.00	0.72	2.86	1.08
$LiMnPO_4$	1.0453 ± 3	0.6098 ± 5	0.4750 ± 6	0.3028 ± 5	1.30	0.91	3.13	1.56
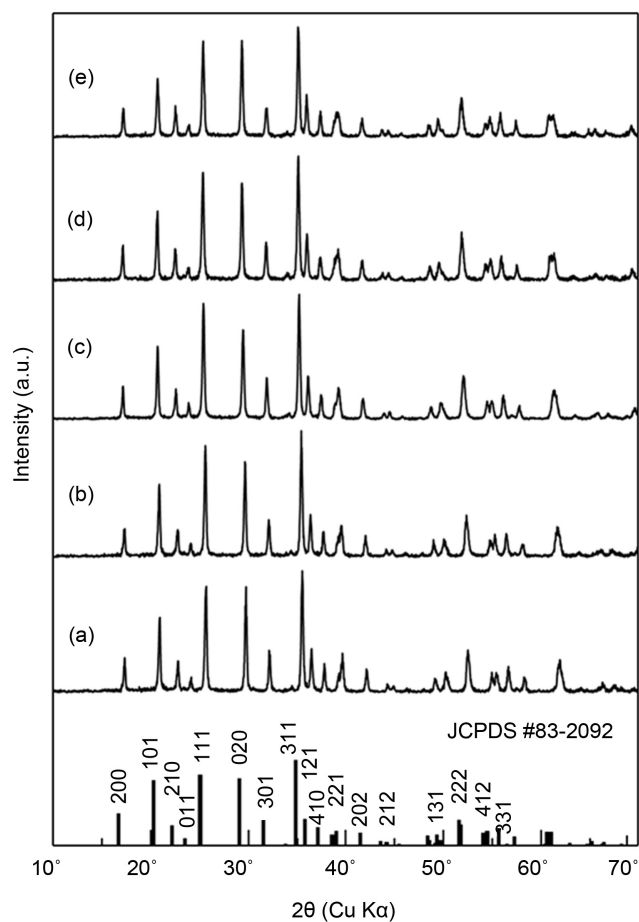
Figure 2. XRD patterns of the products synthesized by hydrothermal process with Mn addition ratio (a) $x = 0$, (b) $x = 0.25$, (c) $x = 0.5$, (d) $x = 0.75$, (e) $x = 1.0$.

of $x = 0$ was $a = 1.0338 \pm 5$ nm, $b = 0.5995 \pm 4$ nm, $c = 0.4696 \pm 1$ nm and $V = 0.2910 \pm 8$ nm^3, and it was a little larger than that of the reported products synthesized by hydrothermal reaction [18]. Its difference was thought because of presence of amorphous phase. In $x = 1.0$, the lattice volume was expanding up to $V = 0.3028 \pm 5$ nm^3. Thus, it was found that the lattice expansion was depended on Mn addition amount for LiMn$_x$Fe$_{1-x}$PO$_4$.

3.3. The Local Structure of Mn Substituted Olivine Material

The local structure of transition metal ion was characterized by XAFS analysis. The valence number of transition metal ion was identified from energy value of the absorption edge, E_0, defined as maximum value of derivative of XANES spectra. E_0 is located in lower energy with smaller valence number, generally. Fe K-edge and MnK-edge XANES spectra were shown in Figure 3. In both spectra of K-edge, with increasing Mn addition amounts, no difference of XANES spectra of the products was observed remarkably. In Fe K-edge XANES spectra, pre-edge peaks attributed to 1s-3d transition was observed at about 7112 eV. Then, E_0 of the products was located in 7119 eV close to that of Fe(II)O. Correspondingly, in MnK-edge, pre-edge peaks and E_0 was observed at 6538 eV and 6546 eV close to that of Mn(II)O, respectively. Therefore, it was thought that iron and manganese ions were existed as divalent ion. Next, the results of radius distribution function furrier transformed of Fe K-edge and MnK-edge EXAFS spectra were shown in Figure 4. As each radius distribution function showed the similar curves, and it was thought that similar local structure was reflected to those curves. Radius distribution function was curve fitted based on the following basic EXAFS formula [21].
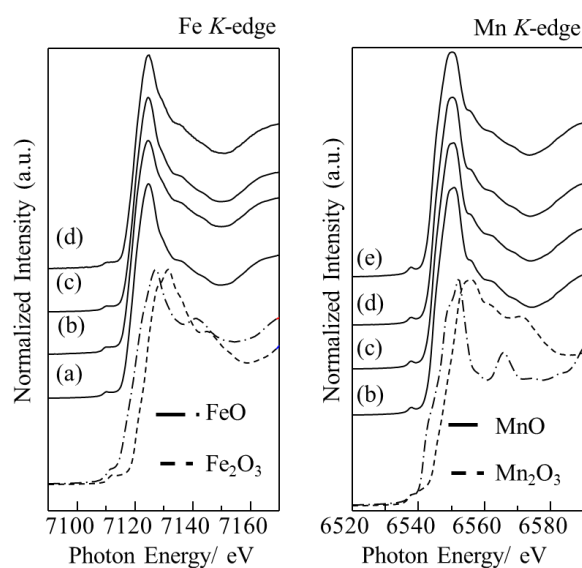
Figure 3. XANES spectra of Fe K-edge and Mn K-edge for the products synthesized by hydrothermal process with Mn addition ratio (a) $x = 0$, (b) $x = 0.25$, (c) $x = 0.50$, (d) $x = 0.75$, (e) $x = 1.0$.
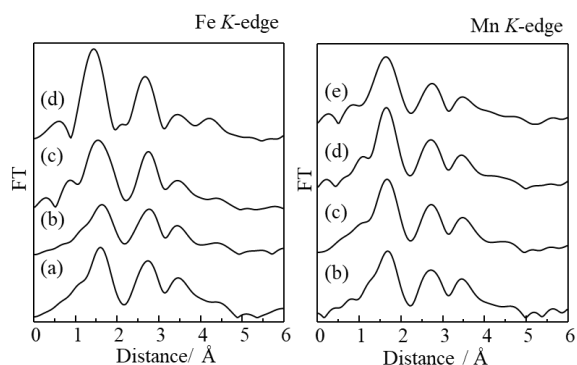
Figure 4. Radius distribution function of Fe K-edge and Mn K-edge for the products synthesized by hydrothermal process with Mn addition ratio (a) $x = 0$, (b) $x = 0.25$, (c) $x = 0.50$, (d) $x = 0.75$, (e) $x = 1.0$.

$$\chi(k) = \sum_j \frac{N_j f_j(k) e^{-2k^2 \sigma_j^2}}{kR_j^2} \sin\left[2kR_j + \delta_j(k)\right] \tag{1}$$

where $f(k)$ and $\delta(k)$ are scattering properties of the atoms neighboring the excited atom, N is the number of neighboring atoms, R is the distance to the neighboring atom, and σ^2 is the disorder in the neighbor distance. The number of coordination atom ($C.\ N.$), the bond distance (R) and the Debye-Waller factor (σ) were shown in Table 3. From olivine-type structural model, the first proximity atom around transition metal ion is oxygen and the second is phosphorus. In Fe K-edge, the first peak was attributed to Fe-O bonds. The estimated coordination number of the first peak was 3 and the bond distance in $x = 0$ was 0.208 nm, and the Debye-Waller factor strongly correlated to the coordination number was 0.098. The obtained coordination number was less than 6 kinds of Fe-O bond distances in FeO_6 octahedra. In A. Yamada's report [10], FeO_6 octahedra with *Pnma* symmetry was distorted and the six Fe-O bond distances were 0.206, 0.206, 0.211, 0.221, 0.225 and 0.225 nm, respectively. The number of Fe-O bonds around 0.21 nm is 3, and it was similar to the calculated value. The other Fe-Obonds in FeO_6 octahedra have about 0.23 nm of the bond distance. The peak separation attributed to these bonds was difficult due to less wave vector range to use for curvefitting. In $LiMn_xFe_{1-x}PO_4$ compounds, Fe-O bond distance was similar value. Corresponding to Fe K-edge, the first peak was attributed to Mn-O bonds in Mn K-edge. The estimated coordination number of the first peak was 3 and the bond distance in $x = 1.0$ was 0.214 nm larger than the Fe-O bond distance. In $LiMn_xFe_{1-x}PO_4$ compounds, Mn-O bond distance was similar value. As a result, it is thought that the Me-O distance unless the Mn addition amount was constant value. MeO_6 octahedra and PO_4 tetrahedra have the structure that a ridge shared one side, so it suggested that the angle provided by these polyhedral would be changed because of Mn addition. The substitution of larger size Mn^{2+} into Fe site might distort the olivine structure, especially the MeO_6 octahedra.

Table 3. The coordination number (C.N.), bond distance (R) and Debye-Waller factor (σ).

	Fe-O			Mn-O		
	C.N.	R/nm	□	C.N.	R/nm	□
$LiFePO_4$	2.7	0.208	0.092	-	-	-
$LiMn_{0.25}Fe_{0.25}PO_4$	2.1	0.211	0.094	3.7	0.214	0.099
$LiMn_{0.5}Fe_{0.5}PO_4$	3.3	0.207	0.106	3.6	0.215	0.086
$LiMn_{0.75}Fe_{0.25}PO_4$	2.4	0.201	0.070	3.7	0.215	0.088
$LiMnPO_4$				3.5	0.214	0.092

3.4. The Vibrational Structure of PO_4 Tetrahedra

The structural distortion by larger MeO_6 octahedra was affected to nearly PO_4 tetrahedral structure. Mn substituted $LiMn_xFe_{1-x}PO_4$ has the PO_4 tetrahedra with infrared absorbency. The vibrational structure of PO_4 tetrahedra was measured by FT-IR, and its spectra were showed in Figure 5. According to Rulmont et al. [22], IR spectra of PO_4 bands were attributed in following. In the case of the products of Mn addition ratio $x = 0$, υ_1 symmetric stretching vibration of P-O was 985.3 cm^{-1}, and υ_3 asymmetric stretching vibrations were 1053.4, 1095.9 and 1138.4 cm^{-1}. In addition, υ_2 symmetric bending of O-P-O was 474.9 cm^{-1}, and υ_4 asymmetric bending was 501.9, 552.9, 578.4 and 635.1 cm^{-1}. With increasing the Mn addition ratio x, a part of absorption band around 1000 cm^{-1} was shifted to blue shift. In $x = 0.25$, absorption band top was 998.1 cm^{-1}, approached to 1009.4 cm^{-1} in $x = 1.0$. The reason of this tendency was why expanded MnO_6 structure was affected to the nearly PO_4 structure. MeO_6 octahedra in the olivine structure occurred the distortion of PO_4 and MeO_6 zig-zag chains.

4. Conclusion

Mn substituted $LiMn_xFe_{1-x}PO_4$ was synthesized by hydrothermal process, and that crystal structure was in detail evaluated. The microstructure of the products was 0.5 μm size particles, and those compounds were provided equally compared to Mn addition amounts by ICP-analysis. XRD results showed that the products were attributed to orthorhombic olivine-type structure. In addition, the diffraction peaks were shifted to low angle with increasing Mn addition amounts, and it suggested that larger size Mn^{2+} was substituted in olivine structure, and expanded the lattice spacing. The structure parameter was refined by Rietveld analysis. The lattice constant in $x = 0$ was $a = 1.0338 \pm 5$ nm, $b = 0.5995 \pm 4$ nm and $c = 0.4696 \pm 1$ nm, and it expanded with increasing Mn addition. The substituted larger size Mn^{2+} might distort the structure of olivine, especially the MeO_6 octahedra. This distortion was confirmed by XAFS analysis. The atom distance of Mn-O was 0.214 nm larger than 0.208 nm of Fe-O. From FTIR, the PO_4 vibrational structure was partly changed, so it was thought that MeO structure expansion was affected to the nearly PO_4 structure.
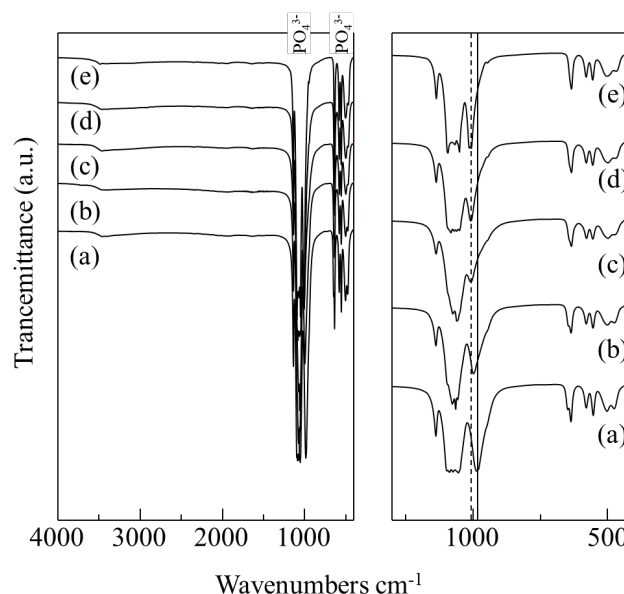
Figure 5. FT-IR spectra of the producta synthesized by hydrothermal process with Mn addition ratio (a) $x = 0$, (b) $x = 0.25$, (c) $x = 0.50$, (d) $x = 0.75$, (e) $x = 1.0$.

Acknowledgements

References

[1] Padhi, A.K., Nanjundaswamy, K.S. and Goodenough, J.B. (1997) Phospho-Olivines as Positive-Electrode Materials for Rechargeable Lithium Batteries. *Journal of Electrochemical Society*, **144** 1188-1194. https://doi.org/10.1149/1.1837571

[2] Delacourt, C., Poizot, P., Morcrette, M., Tarascon, J.M. and Masquelier, C. (2004) One-Step Low-Temperature Route for the Preparation of Electrochemically Active $LiMnPO_4$ Powders. *Chemistry of Materials*, **16**, 93-99. https://doi.org/10.1021/cm030347b

[3] Morgan, D., Van der Ven, A. and Ceder, G. (2004) Li Conductivity in Li_xMPO_4 (M = Mn, Fe, Co, Ni) Olivine Materials. *Electrochemical and Solid-State Letters*, **7**, A30-A32. https://doi.org/10.1149/1.1633511

[4] Chung, S.-Y., Blocking, J.T. and Chiang, Y.-M. (2002) Electronically Conductive Phosphor-Olivines as Lithium Storage Electrodes. *Nature Materials*, **1**, 123-128. https://doi.org/10.1038/nmat732

[5] Shiratsuchi, T., Shigeto, O., Takayuki, D. and Yamaki, J. (2009) Cathodic Performance of $LiMn_{1-x}M_xPO_4$ (M = Ti, Mg and Zr) Annealed in an Inert Atmosphere. *Electrochimica Acta*, **54**, 3145-3151. https://doi.org/10.1016/j.electacta.2008.11.069

[6] Fang, H., Yi, H., Hu, C., Yang, B., Yao, Y., Ma, W. and Dai, Y. (2012) Effect of Zn Doping on the Performance of $LiMnPO_4$ Cathode for Lithium Ion Battery. *Electrochimica Acta*, **71**, 266-269. https://doi.org/10.1016/j.electacta.2012.03.160

[7] Wang, D., Ouyang, C., Drézen, T., Exnar, I., Kay, A., Kwon, N., Gouerec, P., Min-

ers, J.H., Wang, M. and Grätzel, M. (2010) Improving the Electrochemical Activity of LiMnPO$_4$ via Mn-Site Substitution. *Journal of Electrochemical Society*, **157**, A225-A229. https://doi.org/10.1149/1.3271112

[8] Nishijima, M., Ootani, T., Kamimura, Y., Sueki, T., Murai, S., Fujita, K., Tanaka, K., Ohira, K., Koyama, Y. and Tanaka, I. (2014) Accelerated Discovery of Cathode Materials with Prolonged Cycle Life for Lithium-Ion Battery. *Nature Communications*, **5**, 4553. https://doi.org/10.1038/ncomms5553

[9] Yamada, A., Kudo, Y. and Liu, K.-Y. (2001) Phase Diagram of Li$_x$(Mn$_y$Fe$_{1-y}$)PO$_4$ (0 $\leqslant x$, $y \leqslant 1$). *Journal of Electrochemical Society*, **148**, A1153-A1158. https://doi.org/10.1149/1.1401083

[10] Yamada, A., Chung, S.C. and Hinokuma, K. (2001) Optimized LiFePO$_4$ for Lithium Battery Cathodes, *Journal of Electrochemical Society*, **148**, A224-A229. https://doi.org/10.1149/1.1348257

[11] Yang, S., Zavalij, P.Y. and Whittingham, M.S. (2001) Hydrothermal Synthesis of Lithium Iron Phosphate Cathodes. *Electrochemistry Communications*, **3**, 505-508. https://doi.org/10.1016/S1388-2481(01)00200-4

[12] Xu, Y., Lu, Y., Yan, L., Tamg, Z. and Yang, R. (2006) Synthesis and Effect of Forming Fe$_2$P Phase on the Physics and Electrochemical Properties of LiFePO$_4$/C Materials. *Journal of Power Sources*, **160**, 570-576. https://doi.org/10.1016/j.jpowsour.2006.01.042

[13] Zhang, Z., Feng, H., Wu, X., Wang, L., Zhang, A., Xia, T., Dong, H. and Liu, M. (2009) One-Step Microwave Synthesis and Characterization of Carbon-Modified Nanocrystalline LiFePO$_4$. *Electrochimica Acta*, **54**, 3206-3210. https://doi.org/10.1016/j.electacta.2008.11.033

[14] Konarova, M. and Taniguchi, J. (2010) Synthesis of Carbon-Coated LiFePO$_4$ Nanoparticles with High Rate Performance in Lithium Secondary Batteries. *Journal of Power Sources*, **195**, 3661-3667. https://doi.org/10.1016/j.jpowsour.2009.11.147

[15] Zaghib, K., Mauger, A., Gendron, F. and Julien, C.M. (2008) Surface Effects on the Physical and Electrochemical Properties of Thin LiFePO$_4$ Particles. *Chemistry of Materials*, **20**, 462-469. https://doi.org/10.1021/cm7027993

[16] Belharouak, I., Johnson, C. and Amine, K. (2005) Synthesis and Electrochemical Analysis of Vapor-Deposited Carbon-Coated LiFePO$_4$. *Electrochemistry Communications*, **7**, 983-988. https://doi.org/10.1016/j.elecom.2005.06.019

[17] Chen, J. and Whittingham, M.S. (2006) Hydrothermal Synthesis of Lithium Iron Phosphate. *Electrochemistry Communications*, **8**, 855-858. https://doi.org/10.1016/j.elecom.2006.03.021

[18] Ou, X., Pan, L., Gu, H., Wu, Y. and Lu, J. (2012) Temperature-Dependent Crystallinity and Morphology of LiFePO$_4$ Prepared by Hydrothermal Synthesis. *Journal of Materials Chemistry*, **22**, 9064-9068. https://doi.org/10.1039/C2JM30191A

[19] Izumi, F. and Momma, K. (2007) Three-Dimensional Visualization in Powder Diffraction. *Solid State Phenomena*, **130**, 15-20. https://doi.org/10.4028/www.scientific.net/SSP.130.15

[20] Shannon, R.D. (1976) Revised Effective Ionic Radii and Systematic Studies of Interatomie Distances in Halides and Chaleogenides. *Acta Crystallographica Section A*, **32**, 751-767. https://doi.org/10.1107/S0567739476001551

[21] Stern, E.A. and Heald, S.M. (1983) Handbook of Synchrotron Radiation, Chapter 10, 995-1014.

[22] Rulmont, A., Cahay, R., Liegeois-Duyckaerts, M. and Tarte, P. (1991) Article title. *Eur. J. Solid Inorg. Chem.*, **28**, 207.

Supporting Information

(a)

(b)

(c)
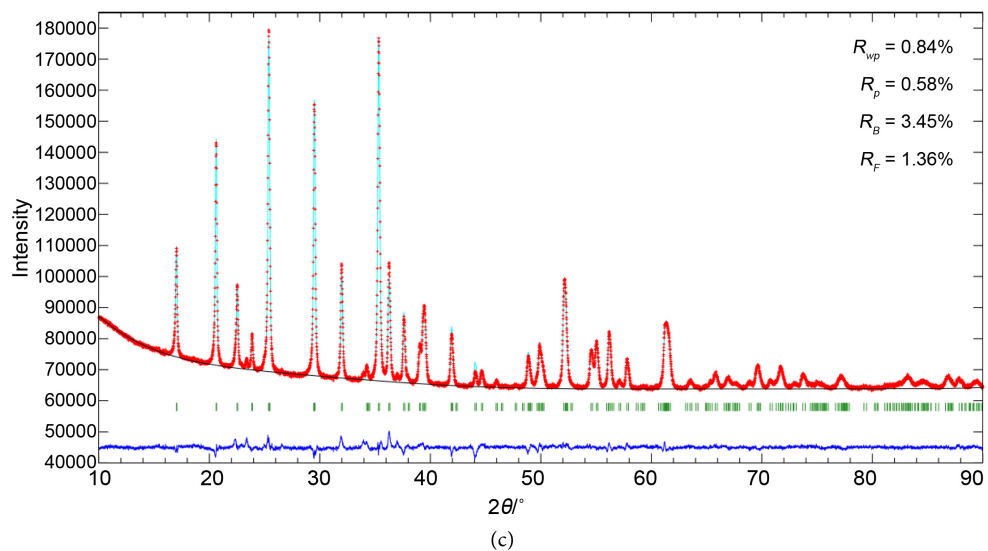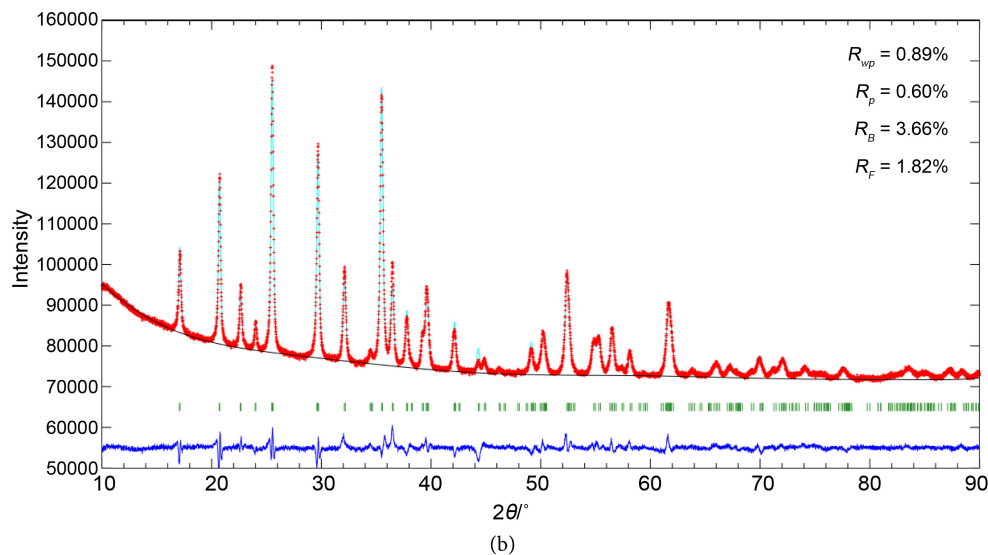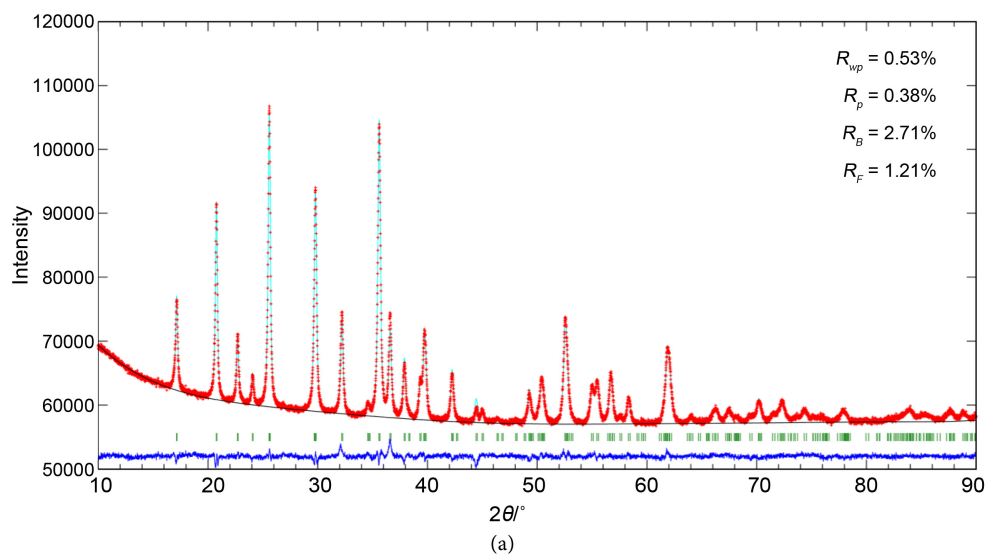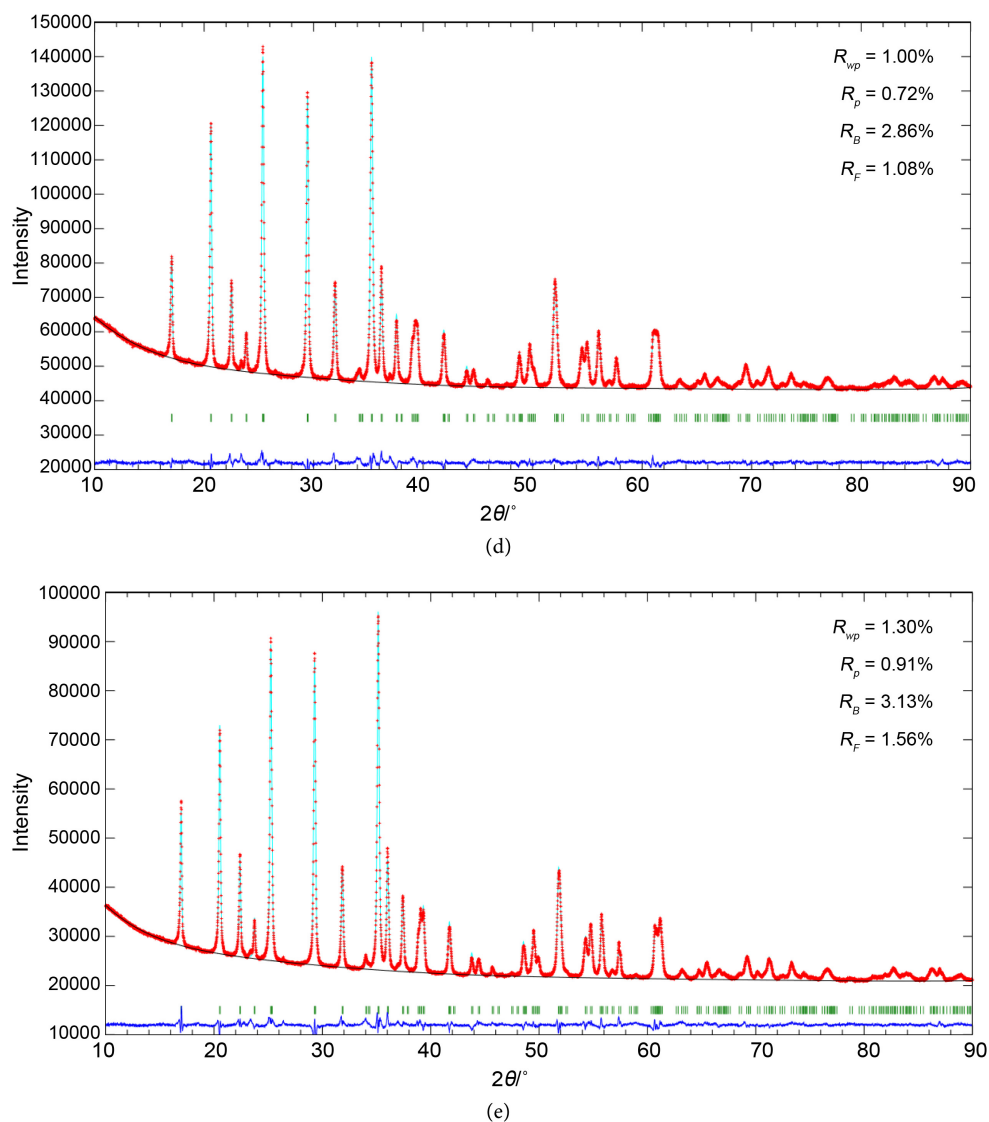
Figure S1. Observed (red), calculated (dark-blue), and difference (blue) refinement patterns resulting from Rietveld analysis. Green vertical bars denote positions of Bragg reflections. (a) LiFePO$_4$, (b) LiMn$_{0.25}$Fe$_{0.75}$PO$_4$, (c) LiMn$_{0.5}$Fe$_{0.5}$PO$_4$, (d) LiMn$_{0.75}$Fe$_{0.25}$PO$_4$, (e) LiMnPO$_4$.